Vibrational Spectroscopy Study of β and α RDX Deposits

Perla Torres, Liza Mercado, Ismael Cotte, Samuel P. Hernández, N. Mina, Alberto Santana, R. Thomas Chamberlain,† Richard Lareau,† and Miguel E. Castro*

Chemical Imaging Center and Center for Chemical Sensor Development, Department of Chemistry, The University of Puerto Rico at Mayagüez, Mayagüez, Puerto Rico 00682

Received: November 4, 2003; In Final Form: March 5, 2004

Deposits of β and α RDX on glass substrates have been examined with optical and Raman microscopy. The measurements reveal significant differences in the morphology and Raman spectra of β and α RDX. Structures that resemble an island, as well as scattered particles, are observed in white light images of β RDX. Well-defined crystals are observed in white light images of α RDX. The spectroscopic signature of these forms of RDX has marked differences in Raman frequencies and relative intensities. The transition from β to α RDX is driven by the amount of RDX deposited. There is a close agreement between measured and calculated vibrational frequencies for β and gas-phase RDX. A poor correlation is found between measured and predicted Raman intensities and depolarization ratios for β and gas-phase RDX, respectively. These differences lead us to conclude that the properties of β and gas phase RDX are markedly different, despite the similarities in the vibrational frequencies.

1. Introduction

There is a growing interest in the development of new technologies and analytical methodology for the detection of trace amounts of explosive materials.[1,2] The possibility of developing miniaturized technologies for Raman and infrared spectroscopy has motivated interest in the use of techniques based on vibrational spectroscopy for explosive characterization and detection.[3] Structural information regarding the explosive can be obtained in addition to quantitative analysis. The application of these techniques to trace explosive detection requires a detailed characterization of chemicals used as explosives and explosive formulations.[4]

Hexahydro-1,3,5-trinitro-s-triazine, better known as RDX, is a powerful secondary explosive that has attracted considerable attention due to its interesting structure and unique properties.[5] The molecule consists of three NO_2 groups bonded to the nitrogen atoms of a triazine ring. RDX exists in two forms in the solid state.[6] These are denominated as the room-temperature stable α phase and the less understood β form.[5] The spatial orientation of the nitro groups is different in α and β RDX. Vibrational spectroscopy,[5] X-ray diffraction,[6] neutron diffraction measurements,[7] and theoretical calculations[8,9] are consistent with a crystal lattice model for α RDX that consists of two molecules interacting by the NO_2 groups in a *Pbca* lattice that contains eight RDX molecules in the unit cell. As a result of these intermolecular interactions, two NO_2 groups are in nearly axial positions while the third NO_2 group is in the equatorial position with respect to the triazine ring. The symmetry of a single RDX molecule in this phase is C_s.[5]

The β RDX form, on the other hand, has a vibrational spectrum that closely resembles that of RDX in the vapor or in acetonitrile and dimethyl sulfoxide solutions.[5] A C_{3v} symmetry has been proposed for RDX in solution.[10] Due to the similarities in the infrared spectra of RDX in solution and for β and gas-phase RDX, the symmetry of RDX is usually taken as C_{3v}.[5,10] Two structures are possible in which RDX has a C_{3v} symmetry, and they differ in the spatial orientation of the NO_2 groups with respect to the triazine ring. Theoretical calculations[9] and electron diffraction experiments[11] for gas-phase RDX are consistent with a structure in which all of the NO_2 groups are in axial positions with respect to the triazine ring.

We have revisited the RDX system as part of our efforts in the development of selective and sensitive sensors for explosive detection. Raman spectroscopy is a very attractive approach for a selective sensor development due to the sensitivity of Raman spectra to phase symmetry. Interpretation of Raman data, however, requires detailed knowledge of the structure and vibrational modes of the phases examined. We have expanded earlier semiempirical,[10,12] molecular mechanics,[13,14] ab initio,[15,16] and nonlocal density functional[9,17] studies by performing theoretical calculations to determine vibrational frequencies and Raman activities and depolarization ratios for gas phase RDX. The agreement between measured and calculated Raman intensities and depolarization ratios is very poor. We found no experimental evidence for strongly polarized Raman bands, which suggests that the molecules in RDX do not have strongly symmetric vibrational modes.

2. Experimental Section

Raman spectra were acquired using a commercial Renishaw RM 2000 Raman microspectrometer with vibrational and white light imaging capabilities. The 514.5 nm line of a Coherent INNOVA 308 Ar^+ ion laser was used as the excitation source for the Raman measurements. RDX was deposited from a 1000 ppm acetonitrile solution, purchased from Cerilliant (Austin, Texas) using a Rainin RM-2 pipet capable of accurately depositing μL of solution (1 μL solution = 1 μg of RDX) in 0.5 μL steps. The solvent was allowed to evaporate at room temperature after the deposition. No signals due to acetonitrile

* To whom correspondence should be addressed. E-mail: mcastro@uprm.edu.

† Visiting scholar. Permanent address: Federal Aviation Administration Technical Center, Atlantic City, NJ 08405.

10.1021/jp0373550 CCC: $27.50
Published on Web 06/08/2004

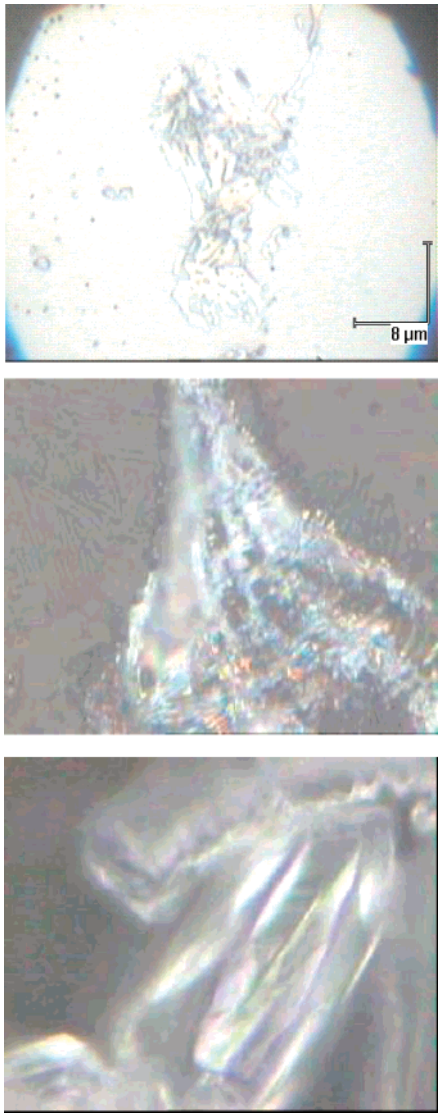

Figure 1. White light images for 0.5 (top), 10 (middle), and 25 μg (bottom) of RDX deposited on a glass substrate.

are observed in the Raman measurements reported here. The white light imaging capabilities of the Reinshaw RM 2000 microscope with magnification factors of 100× or 50× in the objective were employed to obtain the images of RDX deposits on the glass substrates. An objective with a magnification factor of 50× was employed in the acquisition of the Raman spectra reported here. Raman intensities reported here have been corrected for instrument transmission and detector sensitivity, determined by comparing the Raman spectrum of aspirin with literature values.[18]

3. Results

3.1. White Light Imaging of RDX Deposits. Representative white light images of deposits prepared from the deposition of 0.5 (top), 10 (middle), and 25 (bottom) μg of RDX on a glass substrate surface are displayed in Figure 1. The field of view of the image obtained for 0.5 μg of deposited RDX on the glass substrate has a width of 45 μm and a height of 35 μm. The image is dominated by a structure that resembles an island. Scattered particles are observed around the "island-like" structure. Within the resolution of the optical microscope employed for the measurements, we estimate that the particles are about 1 μm in size. Island-like structures are also observed in white

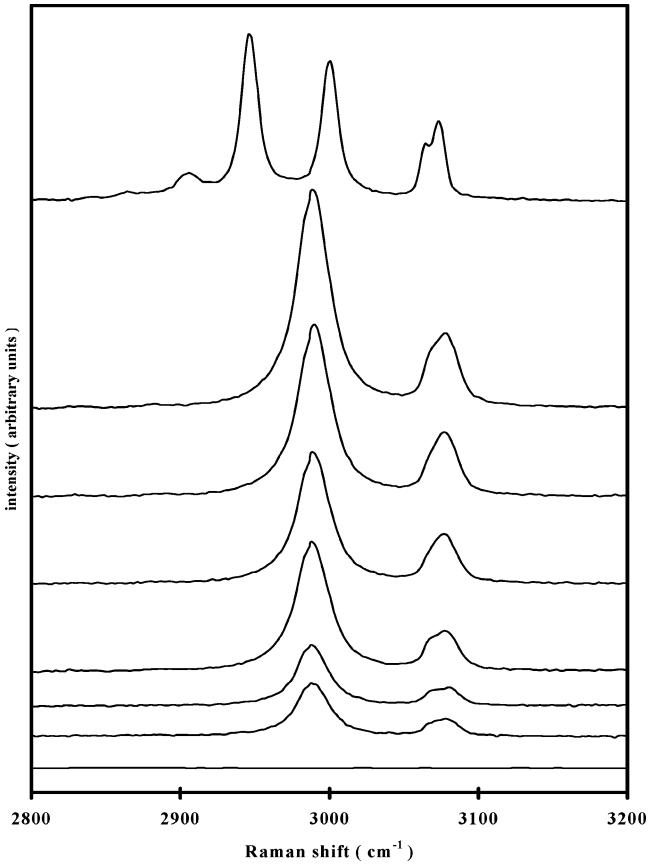

Figure 2. Raman spectra as a function of the amount of deposited RDX on a glass slide. The amounts of deposited RDX, from bottom to top, are: 0, 0.5, 1, 3, 5, 7, 9, and 11 μg.

light images of 10 μg of RDX deposited on a glass substrate. The width and height of the field of view in the image captured for samples prepared by the deposition of 10 μg of RDX on the glass substrate are 100 and 125 μm, respectively. Scattered particles can be distinguished inside the island-like structure displayed in the figure; within the resolution of the optical microscope employed, we estimate that the particles are about 5 μm in diameter, slightly larger than the particles observed in images that correspond to smaller amounts of deposited RDX. Crystallites of various sizes are clearly identified in the images obtained after the deposition of 25 μg of RDX. Crystallites such as those shown on the bottom of Figure 1 are observed in white light images of deposits that have RDX amounts equal to or larger than 11 and up to 25 μg.

3.2. Backscattering Raman Measurements. Backscattering Raman spectra between 2890 and 3200 cm^{-1} and from 150 to 1800 cm^{-1} as a function of the amount of RDX deposited on a glass substrate are summarized in Figures 2 and 3, respectively. Representative Raman spectra of the glass substrates used in the work reported here are displayed in Figures 2 and 3. The glass substrate spectrum has been multiplied by a factor of 0.25 to fit it in the scale with the other spectra shown on the figures. Only broad signals at 1113 and 581 cm^{-1} are observed in Raman measurements of the glass substrate (bottom trace). These signals are readily attenuated after the deposition of 0.5 μg of RDX on the substrate.

Raman signals can be identified in the symmetric and asymmetric C−H bond-stretching region shown in Figure 2. These signals are centered at 2982, 2989, 3068, and 3077 cm^{-1} in the Raman spectrum obtained after the deposition of 0.5 μg of RDX on the glass substrate. A number of bands are observed

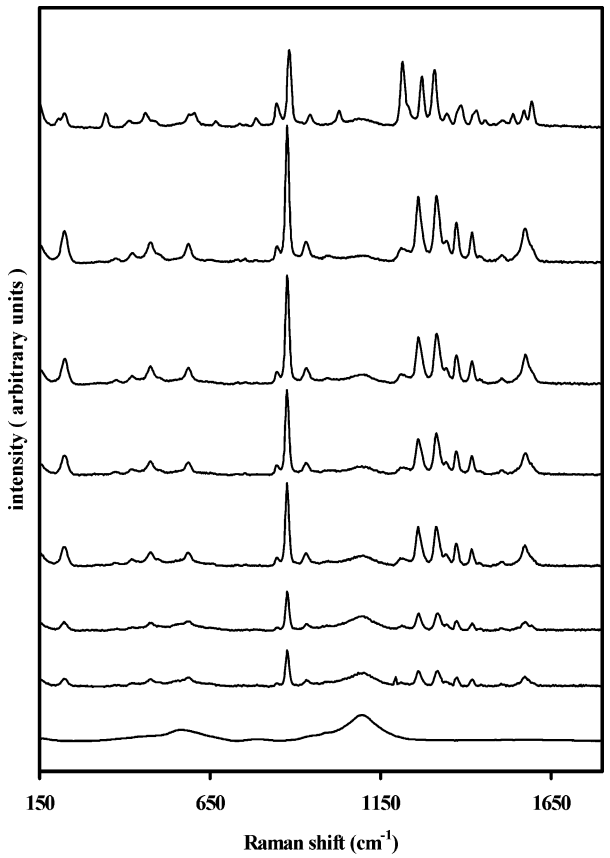

Figure 3. Raman spectra as a function of the amount of deposited RDX on a glass slide. The amounts of deposited RDX, from bottom to top, are: 0, 0.5, 1, 3, 5, 7, 9, and 11 μg.

between 150 and 1800 cm^{-1}. The broad band centered at 1575 cm^{-1} has high and low wavenumber shoulders at 1591 and 1548 cm^{-1}. Bands in this region have been assigned to the NO_2 asymmetric stretch in nitro amines.[20,21] In the closely related octahydro-1,3,5,7-tetranitro-1,3,5,7-tetrazocine, better known as HMX, asymmetric NO_2 stretches are reported between 1500 and 1600 cm^{-1}.[25,31] In 2,4,6-trinitrotoluene (TNT), bands due to asymmetric NO_2 stretching modes are found between 1530 and 1620 cm^{-1}.[30]

The Raman spectrum is complicated between 1500 and 1000 cm^{-1}. Methylene deformation modes are observed between 1445 and 1340 cm^{-1}. Assignment of the bands observed below 1340 cm^{-1} is more complicated. Previous theoretical calculations predict NO_2 deformations and stretches coupled to C−H and N−N and C−N−C deformations between 1300 and 1000 cm^{-1}.[9] This range is consistent with similar vibrational modes in related compounds. For instance, symmetric NO_2 stretches are observed between 1395 and 1345 cm^{-1} in nitro alkanes and can be found between 1365 and 1290 cm^{-1} in the case of nitro amines.[21] In 2,4-dinitrotoluene (DNT) and TNT, bands due to symmetric NO_2 deformation modes are found between 1350 and 1400 cm^{-1}.[29,30] The N−N bond stretch has been reported at 1111 cm^{-1} in the case of hydrazine and at 1225 cm^{-1} in other nitro amines, including HMX.[21,25,31] No evidence was found for a N−N double bond in our measurements, which is found in azomethane at frequencies as high as 1573 cm^{-1}.[21]

The strong Raman peak centered at 878 cm^{-1} is attributed to the symmetric ring-breathing mode. The position of the ring breathing frequency has been traditionally used as an indication of ring strain. For cyclopropane and cyclobutane, the ring breathing frequency is centered at 1188 and 1005 cm^{-1}, respectively.[21] It is located at about 888 cm^{-1} in cyclopentane and at 801 cm^{-1} in cyclohexane.[21] For RDX, we found that the ring breathing frequency is about 77 cm^{-1} higher than in the chair form of cyclohexane. The evidence for ring strain suggests that intramolecular or intermolecular interactions may be important in the properties of RDX. Raman bands between 200 and 800 cm^{-1} have been discussed by a number of investigators in terms of NO_2 deformation and ring torsion modes in the spectrum of bulk RDX and related nitro amine compounds.[5,9,13,14,26,29−31]

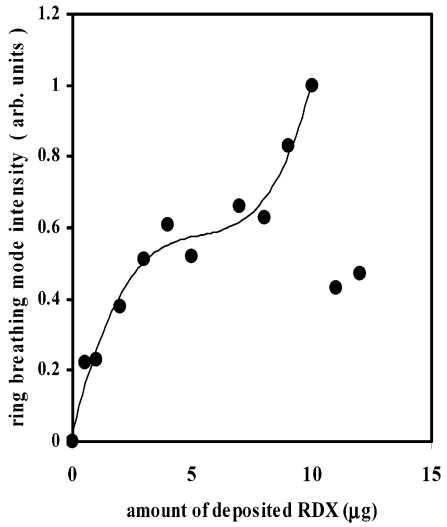

Figure 4. Ring breathing mode intensity as a function of the amount of deposited RDX (in μg) on a glass slide.

The Raman frequencies shift slightly toward lower frequencies, and the corresponding intensities increase with the amount of deposited RDX up to about 10 μg. Changes are observed in the pattern of signals in the Raman spectra when the amount of deposited RDX reaches 11 μg. Multiple bands in the C−H stretching region at 3073, 3064, 3000, 2948, and 2906 cm^{-1} are clearly identified in the spectrum. The broad Raman peaks in the N−O stretching region split into three well resolved peaks at 1594, 1573, and 1555 cm^{-1}. The structure of the Raman spectrum between 1000 and 1500 cm^{-1} is significantly altered. Bands due to methylene and NO_2 deformation modes found between 1350 and 1500 cm^{-1}, for instance, are split into a number of broad bands with shoulders at 1348, 1372, 1385, 1423, 1434, and 1460 cm^{-1}. The N−N stretching mode at 1227 cm^{-1} is one of the strongest peaks between 1000 and 1500 cm^{-1} in the Raman spectrum obtained for amounts of deposited RDX equal or larger than 11 μg, whereas it is just a small shoulder in the Raman spectra measured for lower amounts of deposited RDX. The ring breathing mode frequency is centered at about 882 cm^{-1} in the Raman spectrum that corresponds to 11 μg of deposited RDX, about 4 cm^{-1} higher than in the spectra obtained for deposits with lower amounts of RDX. Raman spectra similar to the one shown for 11 μg of RDX in Figures 2 and 3 have been obtained in this laboratory for amounts of RDX deposited on glass substrates as high as 25 μg.

The dependence of the ring breathing mode signal intensity on the amount of deposited RDX is illustrated in Figure 4. The ring breathing mode signal intensity increases with the amount of RDX deposited on the glass substrate up to about 10 μg. There is a sharp decrease in the ring breathing mode peak intensity above this amount of deposited RDX on the glass substrate. The frequency of the ring breathing and asymmetric NO_2 stretching modes for amounts of deposited RDX equal or smaller than 10 μg is in agreement with values reported for these bands in previous vibrational spectroscopy measurements

TABLE 1: Measured Raman Frequencies, Relative Intensities, and Depolarization Ratios for 2 μg of RDX Deposited on a Glass Substrate

Raman frequency (cm^{-1})	relative Raman intensity	depolarization ratio	tentative assignment[c,d]
227.3	2.42	0.78	
376.8	0.22	*b*	C−N−C deformation[d]
424.2	0.42	0.96	ring breathing[d]
479.7	0.89	0.62	
504.3	0.03	0.76	
588.8	0.93	0.89	
657.5	0.06	*b*	
733.0	0.11	*b*	C−N−C deformation[d]
754.7	0.15	0.68	
787.5	0.04	*a*	ring stretching/ N−O deformation[c] Ring stretching/ N−O deformation[c]
849.0	0.64	*a*	CH_2 rocking and C−N−C deformation[d]
878.8	7.50	0.69	ring breathing[c]
932.8	0.72	0.86	ring stretching/ N−O deformation[c]
996.7	0.02	0.80	ring stretching[c] N−N and ring stretching[c]
1211.1	0.28	*a,b*	CH_2 wagging[d] N−O stretching[c]
1261.4	2.23	*a*	CH_2 scissoring N−N stretch[d]
1271.9	0.90	*a*	N−O stretching[c] N−O stretching[c]
1314.2	1.98	0.72	CH_2 wagging[d]
1343.2	0.26	*a, b*	N−O stretching[c] N−O stretching[c]
1373.8	1.34	0.89	CH_2 scissoring[d]
1419.5	1.11	0.72	C−H skeletal[c]
1442.7	0.10	0.76	C−H skeletal[c]
1507.2	0.17	0.64	N−O stretching[c]
1547.9	0.19	*b*	N−O stretching
1574.3	1.00	*b*	N−O stretching
1590.9	1.04	*b*	N−O stretching
2987.0	2.65	0.83	C−H stretching
3066.5	0.10	*a*	C−H stretching
3075.1	0.21	0.69	C−H stretching

[a] Peak is part of non resolved band. [b] Poor signal-to-noise ratio does not allow for an accurate measurement of depolarization ratio. [c] Indicates assignments from ref 5. [d] Refers to this work.

on β RDX deposits.[5] On the other hand, the frequency of the NO_2 stretching, ring breathing, and N−N stretching modes for amounts of deposited RDX equal or larger than 11 μg are in agreement with the vibrational spectra reported in the literature for α and bulk RDX.[5] The difference in the morphology of the RDX deposits is also consistent with reported observations based on optical microscopy of β and α RDX.[6] Based on the arguments presented above, we attribute the white light images and Raman spectra obtained for amounts of deposited RDX equal or smaller than 10 μg to the β form of the material. The Raman spectra and white light images obtained for amounts of deposited RDX equal to or larger than 11 μg are attributed to α RDX. The abrupt change observed in the ring breathing mode signal intensity in going from 10 to 11 μg of deposited RDX is attributed to a β to α RDX transformation. This transition is sensitive to the amount of RDX deposited, as evidenced by the dependence of the ring breathing mode intensity on the amount of deposited RDX.

Table 1 summarizes the Raman frequencies and relative Raman intensities obtained in this work after the deposition of 2 μg of RDX on the glass substrate. β RDX is the only form observed when this amount of material is deposited. The Raman intensities summarized in Table 1 have been corrected for instrument response and are normalized to the intensity of the NO_2 asymmetric stretching mode at 1574 cm^{-1}. Results of measurements of the depolarization ratios (ρ) are also summarized in Table 1. The component of the backscattered Raman intensity parallel ($I_{||}$) to the plane that contains the electric field of the incident radiation was measured after the backscattered light was filtered thru a polarizer. The component of the backscattered Raman intensity perpendicular ($I_{\perp}$) to the plane that contains the electric field of the incident radiation was measured after the backscattered light was rotated with a halfway plate and then filtered thru a polarizer. Depolarization ratios summarized in Table 1 represent the $I_{||}/I_{\perp}$ intensities ratio. Values of depolarization ratios for β RDX are between 0.6 and 0.96. We found no evidence for strongly polarized vibrational modes in β RDX. In passing, we note that measurements of the depolarization ratios for α RDX were also performed. We found a number of polarized bands, with depolarization ratios below 0.75. For instance, a depolarization ratio of 0.30 was found for the ring-breathing mode in α RDX under identical experimental conditions as those employed in the measurements for β RDX. The Raman spectrum and depolarization ratios of bulk RDX have been studied in detail elsewhere and will not be discussed here.[13,14,27]

3.3. DFT Calculations. Table 2 summarizes nonscaled vibrational frequencies, Raman activities, and depolarization rations (ρ) obtained from density functional calculations (DFT) at the B3LYP/6-311++G** and B3LYP/6-311+G** levels for gas-phase RDX. DFT calculations were performed using the Gaussian 98 (Gaussian, Inc., Pittsburgh, PA) package.[19]

The structure that results from the calculations at both levels of theory has all NO_2 groups in axial position with respect to a chair conformation of the triazine ring. The frequencies calculated at the B3LYP/6-311++G** and B3LYP/6-311+G** have similar values in most of the modes. Infrared intensities (not shown) found in this work are consistent with those reported earlier by Rice and Chabalowski for the RDX isomer with all of the NO_2 groups in axial position with respect to the triazine ring at the B3LYP/6-311+G**.[9] These authors have presented a strong case to correlate calculated and measured vibrational frequencies and pattern of peak intensities of this RDX isomer with gas phase and β RDX.[9] The work presented here extends earlier theoretical work to include Raman activities and depolarization ratios. The calculations predict a C−H stretching mode to have the highest Raman activity and 30 of the 57 normal modes to have depolarization ratios below 0.75. The calculations predict the frequency of the symmetric ring-breathing mode at 936 cm^{-1}. This value is only about 6% higher than the value determined from our measurements for the ring-breathing mode in β RDX.

4. Discussion

The selectivity and sensitivity of Raman spectroscopy for the characterization of explosive material is readily evidenced in the measurements presented here for β and α RDX. The morphology of these two forms is very different, as evidenced in the white light images obtained for β and α RDX. Patches that resemble an island, as well as scattered particles, are readily observed in the white light images of β RDX, wheras well-defined crystals are seen in the α RDX images. Our interpretation of the RDX images in terms of two forms is in agreement with results from optical microscopy observations reported by McCrone nearly fifty years ago.[6] The Raman spectra displayed on Figures 2 and 3 provide stronger evidence to the interpretation of white light images discussed above. The ring-breathing

TABLE 2: Calculated Frequencies, Raman Activities, and Depolarization Ratios

6-311+G**			6-311++G**		
freq. (cm^{-1})	Raman activity	depolarization ratio	freq. (cm^{-1})	Raman activity	depolarization ratio
3193	45	0.31	3193	45	0.30
3190	14	0.45	3190	13	0.45
3190	7	0.74	3190	7	0.73
3069	320	0.12	3069	322	0.12
3064	31	0.41	3064	31	0.41
3062	28	0.48	3062	28	0.49
1658	8	0.75	1658	8	0.75
1657	8	0.75	1657	8	0.75
1627	0	0.74	1627	0	0.74
1483	1	0.04	1483	1	0.02
1466	9	0.75	1466	9	0.75
1465	8	0.75	1465	9	0.75
1403	3	0.75	1403	3	0.75
1402	4	0.75	1402	4	0.75
1383	5	0.75	1383	5	0.75
1381	4	0.75	1381	4	0.75
1363	0	0.60	1362	0	0.58
1345	22	0.08	1345	22	0.08
1294	10	0.75	1294	10	0.75
1292	10	0.75	1291	10	0.75
1274	0	0.73	1274	0	0.74
1253	2	0.75	1253	2	0.75
1251	2	0.75	1251	2	0.75
1244	6	0.02	1244	6	0.02
1143	0	0.70	1143	0	0.70
1007	2	0.74	1007	2	0.74
1006	2	0.75	1006	2	0.75
936	13	0.02	936	13	0.02
909	1	0.75	909	1	0.75
907	1	0.69	907	1	0.69
887	29	0.02	887	29	0.02
863	1	0.75	863	1	0.75
863	1	0.75	863	1	0.75
780	1	0.52	780	1	0.50
753	0	0.73	754	0	0.73
752	0	0.70	752	0	0.70
751	0	0.73	751	0	0.73
661	0	0.73	661	0	0.73
659	0	0.74	659	0	0.74
595	0	0.75	595	0	0.75
592	4	0.75	592	4	0.75
590	4	0.75	590	4	0.75
455	6	0.05	455	6	0.05
439	5	0.00	439	6	0.00
408	1	0.75	408	1	0.75
406	1	0.75	405	1	0.75
362	0	0.73	362	0	0.73
361	0	0.72	361	0	0.72
304	0	0.74	304	0	0.74
219	2	0.75	219	2	0.75
215	2	0.75	215	2	0.75
100	1	0.75	100	1	0.75
99	1	0.75	99	1	0.75
65	0	0.55	65	0	0.62
64	3	0.51	63	4	0.50
35	3	0.75	34	3	0.75
31	3	0.75	31	3	0.75

mode in RDX is reported at 878 cm^{-1}, in agreement with our measurements for amounts of deposited RDX smaller than 10 μg.[5] The poorly resolved structure of vibrational bands between 1500 and 1600 cm^{-1} observed here for amounts of deposited RDX equal to or smaller than 10 μg has been observed in the infrared spectrum of β RDX and RDX in solution and discussed in terms of NO_2 stretching modes.[5,10] A ring breathing mode frequency between 882 and 884 cm^{-1} for α RDX has been reported by various investigators.[5,14] The intense band due to the N−N stretching mode centered at 1227 cm^{-1} and the three well resolved bands between 1500 and 1600 cm^{-1} due to NO_2 stretching modes are characteristic of the vibrational spectra reported in the literature for α and bulk RDX.[5,25,26] The marked splitting of bands between 2900 and 3100 cm^{-1} observed in the Raman spectrum for 11 μg of deposited RDX has been observed in measurements of RDX in the form of powder.[10,25,26]

Karpowicz and Brill have previously measured the infrared spectra of several phases of RDX.[5] These authors measured the infrared spectrum of RDX in the vapor, solution, and β and α forms.[5] The intensity and frequency of modes in the infrared spectra of β and vapor phase RDX were found to be remarkably similar. These results lead to the conclusion of similar symmetries of β and vapor phase RDX. In the context of this model, the increase in the number of Raman signals in going from β to α RDX has traditionally being discussed in terms of a decrease in symmetry from C_{3v} to C_s. A similar difference in symmetry has been inferred from infrared and Raman measurements of RDX in the form of powder (C_s) and in dimethyl sulfoxide solutions, where it has been proposed to have a C_{3v} symmetry.[5,10]

In the context of the Karpowicz and Brill model, the decrease in symmetry from C_{3v} to C_s is consistent with the appearance of doublets of the A′ and A″ type in C_s symmetry.[5] The ring-breathing mode, for instance, that appears as a single band in the spectrum of the β form at 878 cm^{-1} is split into a doublet at 849 and 884 cm^{-1} in the spectrum of the α phase. Further support for this model is also observed in the methylene-stretching region. For instance, the methylene C−H bond stretching band observed at about 2989 cm^{-1} in the spectrum of β RDX is split into a doublet at 2948 and 3001 cm^{-1} in the spectrum of α RDX.

The vapor pressure of RDX is of the order of 10^{-9} Torr.[23] Such a low vapor pressure precluded reliable measurements of the Raman spectrum and depolarization ratios for gas-phase RDX. In the elegant work of Rice and Chabalowski, an excellent agreement was found between the calculated and measured infrared spectrum of gas phase and β RDX, respectively. These authors found a very good correlation in the peak intensity pattern and frequencies of the infrared spectra for gas phase and β RDX with the theoretical predictions for the RDX isomer with all NO_2 groups in axial position.[9] The calculations presented here, at the same level of theory as those performed by the above authors, allow us to compare predicted and measured frequencies and intensities in the Raman spectra of the gas-phase RDX isomer with all NO_2 groups in axial position and β RDX, respectively.

The close agreement between the experimental and calculated Raman frequencies is consistent with the proposal that gas phase and β RDX have all NO_2 groups in the axial position with respect to the triazine ring. The agreement in the relative Raman activities and depolarization ratios is, however, very poor. The calculations predict one of the symmetric C−H stretching modes to have the strongest Raman activity. The measurements presented here indicate that the symmetric ring-breathing mode at 878 cm^{-1} is the strongest peak in the Raman spectrum of β RDX.

Depolarization ratios (ρ) are defined as the ratio of the intensity of the perpendicular ($I_\perp$) to the intensity of the parallel ($I_\parallel$) component of the scattered radiation according to

$$\rho = 3\gamma'^2/[45\alpha'^2 + 4\gamma'^2] \quad (1)$$

where α' and γ' represent the isotropic and anisotropic part of the polarizability change resulting from a normal vibration.[20] Nonsymmetric vibrations have α' equal to zero and a depolar-

ization ratio equal to 0.75.[20] Raman active modes of high symmetry have non-zero values of the isotropic polarizability change (α'), resulting in depolarization values between 0 and 0.75.[20] Highly symmetric modes have very small depolarization ratios. For example, the symmetric Au−Cl bond stretch in $AuCl_4^-$ and the symmetric C−Cl bond stretch in CCl_4 have depolarization ratios of 0.08 and 0.03, respectively. Symmetric modes in larger molecules or chemical systems also have small depolarization ratios. The totally symmetric Ag mode in C_{60}, for instance, has a depolarization ratio close to zero.[32] The small depolarization ratio found in these polarized modes is due to the nonzero values of the isotropic polarizability change. Higher depolarization ratios, on the other hand, indicate a low symmetry of a specific mode. For example, the asymmetric Au−Cl and C−Cl stretching and deformation modes have depolarization ratios equal to 0.75.[20−22] $AuCl_4^-$ and CCl_4 belong to the D_{4h} and T_{4h} point group, respectively, and are considered molecules of high symmetry.[20−22] Thus, depolarization ratios are not indicative of molecular symmetry. Rather, their magnitude can be associated with the symmetry of a vibrational mode. Only eight polarized bands, with depolarization ratios between 0.69 and 0.74, are found in the measurements performed on β RDX. Depolarization ratios between 0.69 and 0.74 have small values of the polarizability change and reflect vibrational modes with low symmetry. Based on the discussion presented above, we conclude that the vibrational modes in β RDX are modes with low symmetry.

Calculated depolarization ratios for RDX are considerably smaller than those determined in the experiments. For instance, depolarization ratios as low as 0.30 are predicted for symmetric C−H stretches, whereas experimentally the lowest depolarization ratio observed in the modes that appear between 2900 and 3100 cm^{-1} is about 0.69. The ring-breathing frequency predicted at 936 cm^{-1} is expected to have a depolarization ratio of 0.02, whereas the experimental ring breathing mode at 878 cm^{-1} has a depolarization ratio of 0.69, more than 30 times larger than predicted by the calculations for gas phase RDX. The larger depolarization ratios found experimentally indicate that the vibrational modes in β RDX are less symmetric than predicted by theory for gas-phase RDX.

The marked difference between measured and calculated Raman activities and depolarization ratios for β RDX and gas phase RDX lead us to conclude that the spectroscopic properties of RDX in both phases are markedly different, despite the similarities in measured vibrational frequencies in infrared and Raman spectroscopy experiments. This is an important matter, as a gas-phase model has been used to describe the vibrational and structural properties of β RDX. This model is too simple to take into account the results presented here. If the model set forth in previous investigations was adequate, then we would have been able to get a closer agreement between calculated and measured Raman activities and depolarization ratios, similar to the excellent agreement found in earlier calculations focused on the infrared absorption spectra, for gas phase and β RDX, respectively.[5]

The reasons for these differences may lie in intermolecular interactions among molecules in β RDX, which are likely to be absent in the gas phase. Strong intermolecular interactions in α RDX are well documented in the literature, whereas their role in β RDX has received less attention.[5,7,8,13,28] We have made several attempts to prepare traces of RDX using a number of experimental approaches, including a RDX in acetonitrile containing aerosol jet.[24] These experiments have resulted in the formation of RDX particles smaller than those observed around and inside the RDX islands imaged for the 0.5 and 10 μg deposits displayed in Figure 1, with diameters between 100 nm and 1 μm. The formation of RDX nanoparticles, as oppose to a thin layer on the substrate surface, is consistent with strong intermolecular interactions among RDX molecules in the β form of the material. These interactions may reduce the symmetry of modes in RDX molecules in the β form, resulting in modes with depolarization ratios larger than those predicted for gas phase RDX. Theoretical work that takes into account intermolecular interactions is needed to fully understand the spectroscopic properties of β RDX.

We have discussed the experimental work presented here in the context of the Karpowicz and Brill model for the condensed phases of RDX. Recent theoretical work on gas-phase RDX has expanded earlier work by Rice and Chabalowski to the calculation of activation energy barriers for the interconversion among the different RDX isomers.[33] In that work, the energy barrier for interconversion among several RDX isomers in the gas phase was calculated to be no higher than 5 kcal/mol.[33] Thus, in the gas phase, rapid interconversion among the different RDX conformers is very likely at room temperature. The energy barrier for the gas-phase conversion of the isomer with all NO_2 groups in the axial position with respect to the triazine ring to the isomer with one NO_2 group in the equatorial position with respect to the triazine ring is less than 1 kcal/mol. As discussed in the previous paragraphs, these isomers can be identified with β and α RDX, respectively. Assuming first-order kinetics and a preexponential factor of the order of 10^{13} s^{-1}, most of the β RDX should have been converted into α RDX in the time scale of the Raman measurements (about 15−30 min). If, on the other hand, equilibrium is established among the two forms of RDX and assuming that the forward and backward reactions follow first-order kinetics with preexponential factors of the same order of magnitudes, then the fractions of β and α RDX are predicted to be 0.4 and 0.6, respectively. With the microscope objective employed in the measurements, we should have observed signals in the Raman spectra for β RDX in α RDX deposits, and vice versa, in the time scale of the experiments. This is not observed in the areas examined indicating that the interconversion rate between β and α RDX is faster in the gas than in the condensed phase. We have observed crystallites with a spectroscopic signature similar to the one reported here for α RDX in aged (days old) deposits that largely consist of β RDX, consistent with the above statement. Thus, differences in the physical chemistry of RDX in the gas and condensed phases are also deduced from the kinetics of interconversion among these two RDX isomers.

Previous works have established α RDX as the stable form of RDX, whereas β RDX is regarded as an unstable form of the material.[5,6] The reasons for the existence of β RDX in trace amounts of the material are open to discussion. A plausible explanation is that the substrate surface serves to stabilize this form of RDX. In this context, we have prepared RDX deposits on a number of substrate surfaces and found that the turning point for the appearance of the α form is sensitive to the substrate employed. The reader is alerted that the surface elemental composition of the substrates employed is unknown, limiting the interpretation of the results in terms of substrate-RDX interactions. Qualitatively, the results support a proposal based on interactions with the substrate surface playing an important role in the physical properties of β RDX. Further speculation is unwarranted until surface sensitive techniques are employed for the characterization of RDX layers on well-defined substrates surfaces.

5. Conclusions

Deposits of β and α RDX have been examined with Raman microscopy. The measurements reveal significant differences in the morphology and Raman spectra of β and α RDX. The differences in the Raman spectra can be used as the spectroscopic signature of these forms of RDX. The transition from β to α RDX is driven by the amount of RDX deposited. There is a close agreement between measured and predicted vibrational frequencies for β and gas-phase RDX, respectively. A poor correlation was found between measured and predicted Raman intensities and depolarization ratios for β and gas-phase RDX, respectively. These differences lead us to conclude that the properties of β and gas phase RDX are markedly different.

Acknowledgment. Financial support from the Federal Aviation Administration under grant number, 99-G-029, and partial support from the Department of Energy PR EPSCoR program and the UPR-Mayaguez Arts and Sciences SEED money program are gratefully acknowledged. The CIC and CCSD operate with grants from the Puerto Rico Infrastructure Development Company (PRIDCO) and the MURI program of the Department of Defense (contract number DAAD 19-02-1-0257), respectively.

References and Notes

(1) Steinfeld, J. I.; Wornhoudt, J. *Annu. Rev. Phys. Chem.* **1998**, *49*, 203.

(2) Kneipp, K.; Wang, Y.; Dasari, R. R.; Feld, M. S.; Gilbert, B. D.; Janni, J.; Steinfeld, J. I. *Spectrochim. Acta A* **1995**, *51*, 2171.

(3) Mercado, A.; Jani, J.; Gilbert, B.; Steinfeld, J. I. *Proceedings of the Second Explosives Detection Technology Symposium and Aviation Security Technology Conference.* **1996**, 91−99.

(4) Janni, J.; Gilbert, B. D.; Field, R. W.; Steinfeld, J. I. *Spectrochem. Acta Part A* **1997**, *53*, 1375.

(5) Karpowicz, R. J.; Brill, T. B. *J. Phys. Chem.* **1984**, *88*, 348.

(6) McCrone, W. C. *Anal. Chem.* **1950**, *22*, 954.

(7) Choi, C. S.; Prince, E. *Acta Crystallogr. Sect. B* **1972**, *28*, 2857.

(8) Kunz, A. B. *Phys. Rev. B* **1996**, *53*, 9733.

(9) Rice, B. M.; Chabalowski, C. F. *J. Phys. Chem. A* **1997**, *101*, 8720.

(10) Filhol, A.; Clement, C.; Forel, M.-T.; Paviot, J.; Rey-Lafon, M.; Richour, G.; Trinquecoste, C.; Cherville, J. *J. Phys. Chem.* **1971**, *75*, 2056.

(11) Shishkov, I. F.; Vilkov, L. V.; Kolonists, M.; Rozsondai, B. *Struct. Chem.* **1991**, *2*, 57.

(12) Orloff, M. K.; Mullen, P. A.; Rauch, F. C. *J. Phys. Chem.* **1970**, *74*, 2189.

(13) Rey-Lafon, M.; Trinquecoste, C.; Cavagnat, R.; Forel, M.-T. *J. Phys. Chem.* **1970**, *68*, 1533.

(14) Trinquecoste, C.; Rey-Lafon, M.; Forel, M. T. *J. Chem. Phys.* **1975**, *72*, 689.

(15) Habibollahzadeh, D.; Grodzicki, M.; Seminario, J. M.; Politzer, P. *J. Phys. Chem.* **1991**, *95*, 7669.

(16) Coffin, J. M.; Newton, S. Q.; Ewbank, J. D.; Schafer, L.; Alsenoy, C. V.; Siam, K. *J. Mol. Struct. (THEOCHEM)* **1991**, *251*, 219.

(17) Wu, C. J.; Fried, L. E. *J. Phys. Chem. A* **1997**, *101*, 8675.

(18) McCreery, R. L. *Raman Spectroscopy for Chemical Analysis*; Wiley and Sons: New York, 2000.

(19) Frisch, M. J.; Trucks, G. W.; Schlegel, H. B.; Scuseria, G. E.; Robb, M. A.; Cheeseman, J. R.; Zakrzewski, V. G.; Montgomery, J. A., Jr.; Stratmann, R. E.; Burant, J. C.; Dapprich, S.; Millam, J. M.; Daniels, A. D.; Kudin, K. N.; Strain, M. C.; Farkas, O.; Tomasi, J.; Barone, V.; Cossi, M.; Cammi, R.; Mennucci, B.; Pomelli, C.; Adamo, C.; Clifford, S.; Ochterski, J.; Petersson, G. A.; Ayala, P. Y.; Cui, Q.; Morokuma, K.; Malick, D. K.; Rabuck, A. D.; Raghavachari, K.; Foresman, J. B.; Cioslowski, J.; Ortiz, J. V.; Stefanov, B. B.; Liu, G.; Liashenko, A.; Piskorz, P.; Komaromi, I.; Gomperts, R.; Martin, R. L.; Fox, D. J.; Keith, T.; Al-Laham, M. A.; Peng, C. Y.; Nanayakkara, A.; Gonzalez, C.; Challacombe, M.; Gill, P. M. W.; Johnson, B. G.; Chen, W.; Wong, M. W.; Andres, J. L.; Head-Gordon, M.; Replogle, E. S.; Pople, J. A. *Gaussian 98*, revision A.6; Gaussian, Inc.: Pittsburgh, PA, 1998.

(20) Long, D. A. *Raman Spectroscopy*; McGraw-Hill: London, 1977.

(21) Lin-Vien, D.; Colthup, N. B.; Fateley, W. G.; Grasselli, J. G. *The Handbook of Infrared and Raman Characteristic Frequencies of Organic Molecules*; Academic Press: San Diego, CA, 1991.

(22) Pan, P.; Wood, S. A. *Geochim. Cosmochim. Ac.* **1991**, *55*, 2365.

(23) Yinon, J.; Zitrin, S. *Modern Methods and Applications in Analysis of Explosives*; Wiley and Sons: West Sussex, England, 1993; p 247.

(24) Torres, P.; Cotte, I.; Mina, N.; Hernandez, S. P.; Chamberlain, R. T.; Garcia, J.; Lareau, R.; Castro, M. E. *Proc. Int. Conf. Comput. Nanosci. Nanotechnol.* **2002**, *2*, 443−446.

(25) Lewis, I. R.; Daniel, N. W.; Griffiths, P. R. *Appl. Spectrosc.* **1997**, *51*, 1854.

(26) Fell, N. F., Jr.; Vanderhoff, J. A.; Pesce-Rodriguez, R. A.; McNesby, K. L. *J. Raman Spectrosc.* **1998**, *29*, 65.

(27) Cheng, C.; Kirkbride, T. E.; Batchelder, D. N.; Lacey, R. J.; Sheldon, T. G. *J. Forensic Sci.* **1995**, *40*, 31.

(28) Sorescu, D. C.; Rice, B. M.; Thompson, D. L. *J. Phys. Chem. B* **1997**, *101*, 798.

(29) Tao, A.; Kim, F.; Hess, C.; Goldberg, J.; He, R.; Sun, Y.; Xia, Y.; Yang, P. *Nano Lett.* **2003**, *3*, 1229.

(30) Clarkson, J.; Smith, W. E.; Batchelder, D. N.; Smith, D. A.; Coats, A. M. *J. Mol. Struct.* **2003**, *648*, 203.

(31) Goetz, F.; Brill, T. B. *J. Phys. Chem.* **1979**, *83*, 340.

(32) Gallagher, S. H.; Armstrong, R. S.; Clucas, W. A.; Lay, P. A.; Reed, C. A. *J. Phys. Chem. A* **1997**, *101*, 2960.

(33) Vladimiroff, T.; Rice, B. M. *J. Phys. Chem. A* **2002**, *106*, 10437.